Window Observables for Benchmarking Parton Distribution Functions

Joe Karpie,[1,*] Christopher J. Monahan,[2,†] Kostas Orginos,[3,1,‡] and Savvas Zafeiropoulos[4,§]
[1]Thomas Jefferson National Accelerator Facility, Newport News, Virginia 23606, USA
[2]Department of Physics, Colorado College, Colorado Springs, Colorado 80903, USA
[3]Physics Department, William & Mary, Williamsburg, Virginia 23187, USA
[4]Aix Marseille Univ., Université de Toulon, CNRS, CPT, Marseille, France

(Received 3 June 2025; revised 20 August 2025; accepted 3 October 2025; published 3 November 2025)

Global analysis of collider and fixed-target experimental data and calculations from lattice quantum chromodynamics (QCD) are used to gain complementary information on the structure of hadrons. We propose novel "window observables" that allow for higher precision cross-validation between the different approaches, a critical step for studies that wish to combine the datasets. Global analyses are limited by the kinematic regions accessible to experiment, particularly in a range of Bjorken-x, and lattice QCD calculations also have limitations requiring extrapolations to obtain the parton distributions. We provide two different window observables that can be defined within a region of x where extrapolations and interpolations in global analyses remain reliable and where lattice QCD results retain sensitivity and precision.

DOI: 10.1103/q6jl-816j

Introduction—Lattice quantum chromodynamics (QCD) is a vital tool for the precision study of particle physics, from quark flavor physics [1] to the muon's anomalous magnetic moment [2]. Recent theoretical and computational developments have also enabled lattice QCD calculations to become increasingly important in the quest to understand the internal structure of hadrons.

Parton distribution functions (PDFs) encode the longitudinal momentum structure of hadrons. The field-theoretic definition of PDFs relies on the hadronic matrix elements of fields at lightlike separations, which cannot be determined directly in Euclidean lattice QCD and must be extracted using indirect approaches. The primary methods for determining PDFs from lattice QCD are based on Mellin moment calculations of matrix elements of local operators or inference of PDFs from matrix elements of nonlocal operators, through short-distance factorization (SDF) [3–5] or large momentum effective theory (LaMET) [6].

Mellin moments correspond to weighted integrals over PDFs, so a potential challenge for robust comparison between phenomenological determinations of PDFs and the low Mellin moments determined from lattice calculations is that experimental data do not cover the entire range of Bjorken-x. A major goal of both the future Electron-Ion Collider [7] and the JLab 22 GeV upgrade [8] is to extend the range of the available data to reduce the extrapolation errors in PDFs, including the challenging case of nucleon quark transversity.

To determine PDFs via SDF or LaMET, nonlocal matrix elements calculated on the lattice must be Fourier transformed, which leads to an inverse problem associated with the incomplete Fourier transform of discrete, noisy data. Various approaches have been proposed to tackle this inverse problem [9–19]. Quantification of the systematic uncertainties associated with each approach is a significant difficulty and requires validation through multiple lattice calculations using various methods.

As a result of this inverse problem, lattice calculations that apply the SDF and LaMET approaches are most sensitive to the larger x region where experimental data may be lacking. The PDF reconstructed from lattice results is highly correlated point by point in x, and, therefore, integrals over x may have significantly higher precision than anticipated from the point-by-point variance. Inspired by the successful use of windows for the hadronic vacuum polarization contribution to the muon's anomalous magnetic moment [20], these difficulties motivate the use of "window observables" defined across a limited region of x from x_- to x_+.

Benchmarking and validation of lattice calculations have been an important feature in flavor physics for two decades [1] and is a necessary step for meaningful comparison between lattice results and experimental determinations of

*Contact author: jkarpie@jlab.org
†Contact author: cjmonahan@coloradocollege.edu
‡Contact author: kostas@wm.edu
§Contact author: savvas.zafeiropoulos@cpt.univ-mrs.fr

Published by the American Physical Society under the terms of the Creative Commons Attribution 4.0 International license. Further distribution of this work must maintain attribution to the author(s) and the published article's title, journal citation, and DOI. Funded by SCOAP³.

hadron structure [21,22]. Window observables provide benchmark quantities that enable quantitative comparison between, and validation of, lattice calculations of x-dependent hadron structure for three reasons. First, window observables enable direct comparison between PDFs extracted from SDF and LaMET and can be calculated across regions of momentum fraction or Ioffe time in which SDF and LaMET are expected to be reliable. Second, window observables provide quantities that can be extracted directly from phenomenological determinations of PDFs over regions of momentum fraction for which the PDFs are well constrained. These quantities can then be compared to window moments determined from SDF and LaMET. Third, window observables account for the large point-by-point correlations in PDFs and provide more precise benchmark quantities than a pointwise comparison between PDFs extracted from different approaches. Even in low x windows, where experimental data exist and lattice results are noisy, the window observables provide meaningful benchmarks, as we demonstrate through the example of the isovector $u-d$ quark transversity.

This Letter is organized as follows. We briefly review parton structure and then propose two benchmark window observables for meaningful quantitative comparison between SDF, LaMET, and global analyses: window moments and Gaussian windows. To demonstrate a practical application of these window observables, we study synthetic data for the isovector $u-d$ quark transversity of the nucleon determined from JAM3D* [23,24] and JAMDiFF [24,25]. These data enable closure tests for the window observables in the SDF framework. We then apply the same procedure to lattice QCD results from [26]. Finally, we summarize and give future prospects.

Parton structure—Parton structure can be extracted from quantities defined in three interrelated spaces, Ioffe time, momentum fraction, and Mellin, each with advantages and disadvantages. The three representations provide complementary approaches to analyzing hadron structure. The LaMET [6] and SDF [4] approaches start from spacelike Ioffe time distributions (ITDs) $\mathcal{M}(\nu,z^2)$, which were studied earlier in the context of "primordial Transverse momentum-dependent distributions" [27]. Experimental processes, described with Bjorken-x and other momentum fractions, are most naturally analyzed with the PDF. Finally, direct lattice QCD calculations of matrix elements of local operators correspond to integer Mellin moments.

Ioffe-time representation The natural field-theoretic starting point is the renormalized matrix element, dubbed the ITD [28],

$$M(\nu,\mu^2)=\frac{1}{n\cdot p}\langle p|\bar{\psi}(z)\not{n}W(z;0)\psi(0)|p\rangle_{\mu^2},\qquad(1)$$

with the quark fields connected by a straight Wilson line W along the lightlike separation $z_\mu=(0_+,z_-,0_T)=z_-n$, with $n^2=0$. The ITD is a function of the Ioffe time $\nu=-p\cdot z$. In the rest frame of the hadron, such as in a fixed-target experiment like deep inelastic scattering, the Ioffe time $\nu=-mt$ is proportional to the probe interaction time, in units of the hadron mass [29].

Within the SDF approach, the spacelike ITD $\mathcal{M}(\nu,z^2)$, with $z_\mu=(0,0,0,z_3)=z_3n$ and $n^2=-1$, is referred to as the pseudo-ITD. The pseudo-ITD is related to the ITD through [4]

$$\mathcal{M}(\nu,z^2)=\int_0^1 du C(u,\mu^2,z^2)M(u\nu,\mu^2)+O(z^2),\qquad(2)$$

where in the parton limit $C(u)=\delta(1-u)$. The matching kernels have been calculated to $O(\alpha_S)$ [30–32] and $O(\alpha_S^2)$ [33].

Momentum fraction representation The PDF, which arises naturally through QCD factorization of select scattering processes [34], is defined as the inverse Fourier transform of the ITD

$$f(x,\mu^2)=\int_{-\infty}^{\infty}\frac{d\nu}{2\pi}e^{-i\nu x}M(\nu,\mu^2)\qquad(3)$$

and can be obtained from the pseudo-ITD through [4,5]

$$\mathcal{M}(\nu,z^2)=\int_{-1}^{1}dxK(x\nu,\mu^2,z^2)f(x,\mu^2)+O(z^2).\qquad(4)$$

The PDF can also be extracted in the LaMET approach through a related matching relation [6,35].

Mellin representation The operator product expansion (OPE) of the operator defining the ITD [34] is

$$\bar{\psi}(z)\not{n}W(z;0)\psi(0)=\sum_n z_{\mu_1}\ldots z_{\mu_n}\bar{\psi}\gamma^{\{\mu_1}D^{\mu_2}\ldots D^{\mu_n\}}\psi,\qquad(5)$$

where $\{\ldots\}$ represents a traceless and symmetric combination of indices. The ITD itself becomes a series in Ioffe time:

$$M(\nu,\mu^2)=\sum_{n=0}^{\infty}\frac{(i\nu)^n}{n!}a_{n+1}(\mu^2),\qquad(6)$$

where $a_n(\mu^2)$ are the reduced matrix elements of the local operators in the OPE, which are directly related to the Mellin moments of the PDF through

$$a_n(\mu^2)=\int_{-1}^{1}dxx^{n-1}f(x,\mu^2).\qquad(7)$$

Alternatively, one can calculate the Mellin moments of the pseudo-PDF from polynomials of ν [36,37] from a similar OPE for the pseudo-ITD [5].

In the rest of this Letter, we suppress the renormalization scale dependence in all quantities.

Window observables In this Letter, we study convolutions of the PDF that constrain the information to a limited region of x. Generically, these are given by

$$W_n(x_\pm) = \int_{-1}^{1} dx w_n(x; x_\pm) f(x). \tag{8}$$

In both examples below, as the magnitude of $|n|$ increases, up to some normalization, the window observables are dominated by the PDFs at a single point $x = x_+$, x_-, or their average. At smaller $|n|$, they represent relatively wider features within the prescribed window (x_-, x_+), and lattice QCD reconstructions will be more precise than the large $|n|$ approximate point-by-point reconstruction.

One example is "window moments"

$$a_n(x_-, x_+) = \int_{x_-}^{x_+} dx\, x^n f(x). \tag{9}$$

The related "truncated moments," defined with $x_+ = 1$, were first introduced in [38,39] and further studied in [40–46]. We focus on moments with positive n, which lose sensitivity to the lower region as n grows. Moments with n negative have decreasing sensitivity to the upper region and give less reliable lattice QCD benchmarks.

We also propose an alternative window observable, which we call "Gaussian windows," defined by the PDF convoluted with a Gaussian localized in x:

$$g_n(x_-, x_+) = \int_{-1}^{1} dx \sqrt{\frac{n^2}{2\pi x_d^2}} \exp\left[-n^2 \frac{(x - x_0)^2}{2x_d^2}\right] f(x), \tag{10}$$

where $x_0 = (x_+ + x_-)/2$ and $x_d = x_+ - x_-$. Increasing $|n|$ tightens the window about the midpoint x_0. As $|n| \to \infty$, the Gaussian window approaches $f(x_0)$. In some cases, such as the analysis of generalized parton distributions, which exhibit a complicated analytic structure at $x = \xi$, it may be useful to work with locally smeared observables like a Gaussian window with $x_0 \approx \xi$ rather than exact point-by-point values.

Both window moments and Gaussian windows can be obtained from direct integration over x or, as described in End Matter, the convolution theorem can be used to recast window observables as integrations in ν. The window observables, therefore, provide an environment in which direct quantitative comparisons between SDF, LaMET, and global phenomenological analyses can be carried out within regions of mutual validity.

Synthetic data study—To test the calculation of the window observables from lattice QCD data, we generate a synthetic dataset from JAM3D* [23,24], shown in Fig. 1. In End Matter, we show the same analysis on the JAMDiFF dataset [24,25]. We study the $u - d$ transversity ITD at $\mu = 2$ GeV, discretized with a unit spacing using $\nu_{\max} = 4$. At this $\nu_{\max}$, the ITD has not converged to zero, but the extraction can be performed provided extrapolation errors are correctly quantified. In End Matter, we show the results with $\nu_{\max} = 10$.

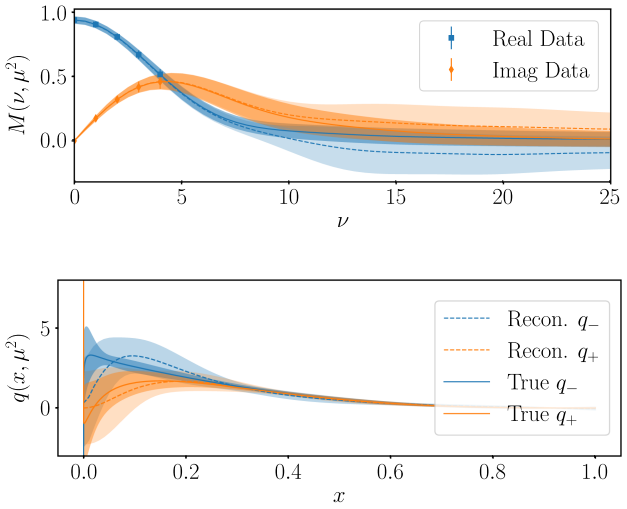


FIG. 1. The GPR of synthetic data from JAM3D*. The GPR reconstruction (dashed line, lighter band) for the *CP*-even (blue) and *CP*-odd (orange) PDFs compared to the original input (solid line, darker band) for (upper) the ITD and (lower) the PDF.

Our numerical analyses utilize the *CP*-projected PDFs, bounded in $x \in [0, 1]$:

$$q_\pm(x) = f(x) \pm -f(-x). \tag{11}$$

This decomposition is convenient because the *CP*-even (q_-) and -odd (q_+) distributions generate, respectively, the real and imaginary components of the ITD.

We first construct a ITD from the JAM3D* dataset and then apply Gaussian process regression (GPR) to infer the PDF from the synthetic ITD data. The implementation follows Ref. [17] except that we use zero as the prior's mean, which drives the extrapolation of the PDF as $x \to 0$. The results are shown in Fig. 1. At all x, the reconstruction systematically overestimates the error of the input, but most dramatically for $x < 0.4$. This may give the misleading impression that any information taken from low x regimes will be similarly inaccurate.

For our example of the window observables, we choose $x_- = 0.1$ within the modern range of Bjorken-x in experimental datasets for the transversity distribution. With $x_- > 0$, we can avoid biases at asymptotically low x in the phenomenological extraction and worse lattice extractions. Although $x_+ = 0.5$ lies above experimentally accessible Bjorken-x, this choice includes a region of x that is still informed by experimental data, due to the convolutions for evolution and matching to cross sections. We expect that this x_+, which is relatively close to the dataset, avoids the worst extrapolation biases that $x_+ \to 1$ could exhibit. We study alternative windows in End Matter.

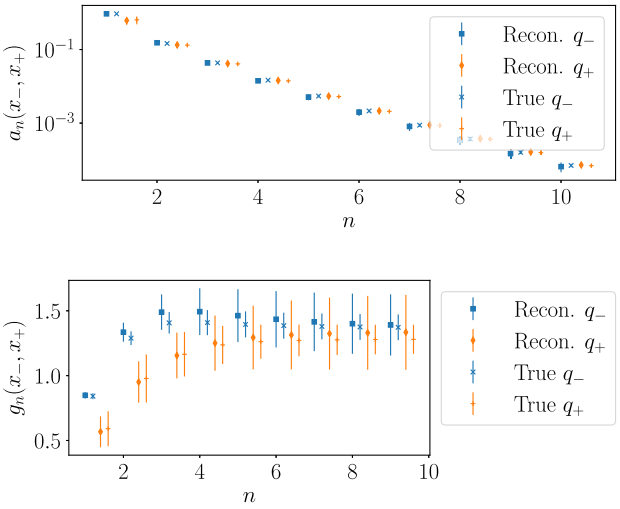


FIG. 2. The window moment (upper) and Gaussian window (lower) with $x_- = 0.1$ and $x_+ = 0.5$.

The reconstructed window observables are compared with the original data in Fig. 2. The relative error of the reconstructions is given in End Matter. Despite the restricted Ioffe time range, the window observables are remarkably accurate, particularly at small n, because the low-ν region is most sensitive to the wider features in x. The increased error of the GPR with respect to the input and the deviation in central value are linked to the extrapolation error, which reduces when $\nu_{\max}$ is increased.

The increased uncertainty of the GPR compared to the input distribution point by point in x does not translate to a similarly sized increase in the errors of the window observables on the lowest n's. The nontrivial covariance in x from the GPR is visually hidden in Fig. 1 but properly accounted for in the integrations of window observables. The correlations between data points incorporate the high precision of low Fourier modes, which impacts the precision of slowing varying features that characterize integrals over a wide region of x.

Therefore, while the overall x reconstruction of the lattice data allows only a broad qualitative statement of agreement due to its overwhelming uncertainty, the window observables with low n provide a much more stringent benchmarking opportunity between lattice data and phenomenological extractions.

Lattice QCD data study—We study window observables using lattice QCD data for the renormalization-group invariant (RGI) ratio of pseudo-ITDs [36] on a single ensemble with lattice spacing $a = 0.094$ fm and pion mass $m_\pi = 358$ MeV, described in detail in [26]. In our analysis of lattice QCD data, we first obtain the CP-projected pseudo-PDFs $P_\pm(x, z^2)$ from lattice data of the spacelike hadronic matrix element using GPR and subsequently match to the PDF. By reducing correlated fluctuations and giving a fixed point at $\nu = 0$, the use of RGI ratios helps constrain the GPR substantially, but, as a consequence, the lattice data differ from the synthetic data study of the previous section by the normalization, g_T. Using the one-loop expression [26], the leading-order (LO) matching and leading-log (LL) evolution are applied to the pseudo-PDF result to obtain the normalized $\overline{\text{MS}}$ PDFs at $\mu = 2$ GeV, shown in Fig. 3 for three z values. Note this nomenclature, which conforms to that typically used in global analyses, is uncommon for lattice QCD studies, which typically denote these NLO and NLO + RGR, respectively. To help control the evolution and matching of the most poorly constrained models for the $x > 0.8$ region, an additional GP prior is added to force the pseudo-PDF to vanish at $x = 1$, with little effect on the low-x window observables. It is clear that the separations suffer from the limited extent in ν. In the imaginary component, the data rise until a peak around $\nu = 5$ and fall off again, but short z, which fail to reach this peak, tend to underestimate its size. Given available momenta, $z = 4a$ is the shortest separation to reach this value. Similar extrapolation biases can more subtly affect the real component.

For comparison to the phenomenological results, the window integrals are multiplied by the g_T normalization obtained from the bare matrix element [47], RI-sMom [48,49] renormalization constant [50], and NNLO matching

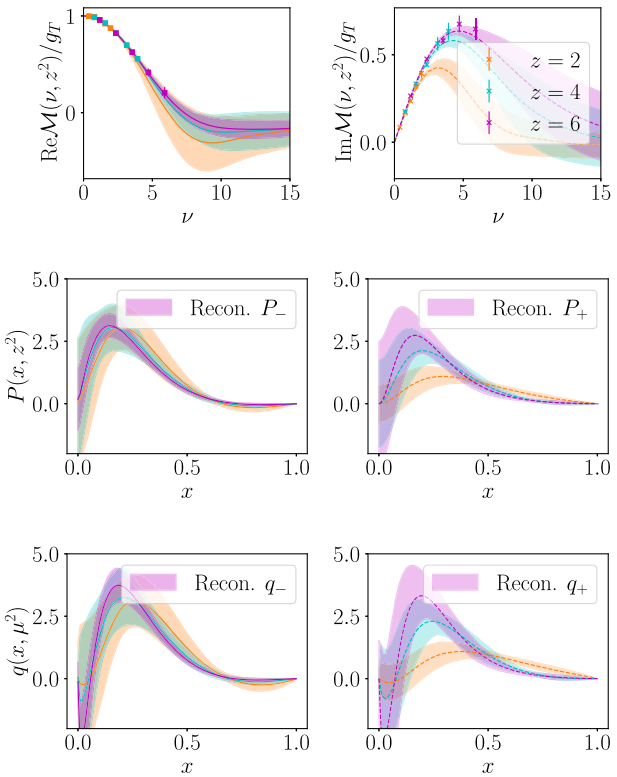


FIG. 3. Upper: the real (squares) and imaginary (crosses) components of the lattice QCD data fit to a GPR. Middle: the CP-even (left) and CP-odd (right) pseudo-PDF reconstructions. Lower: the PDF at $\mu = 2$ GeV resulting from LO matching and LL evolution.

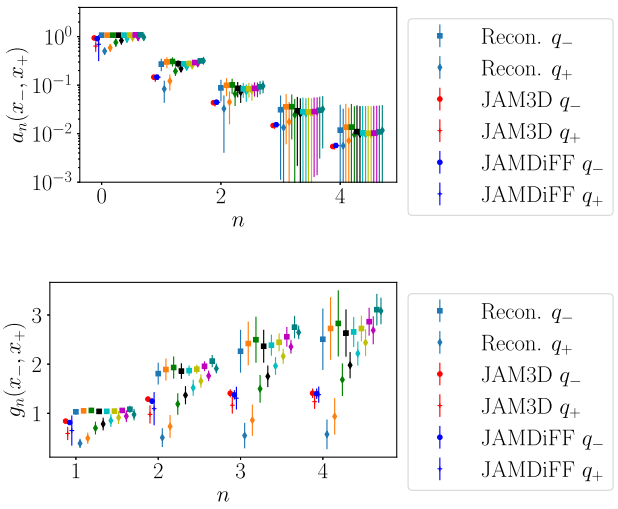


FIG. 4. The window moment (upper) and Gaussian window (lower) with $x_- = 0.1$ and $x_+ = 0.5$. The lattice QCD data for q_- (squares) and q_+ (diamonds) are given with increasing z/a in the range [1, 8] from left to right.

to $\overline{\text{MS}}$ scheme [51,52]. We show the window observables in Fig. 4. They are generally of the same size with an upward trend with z, particularly the Gaussian window. The errors also tend to decrease slightly as z increases, because the larger Ioffe-time extent leads to more constrained reconstructions within the window.

Future study with many ensembles is required to disentangle the effects from discretization, quark mass, higher twist, higher-order perturbation theory, and GP reconstruction error which all contribute to this residual z dependence and cause discrepancies with phenomenology. These limitations are precisely what hinders point-by-point comparison in x, but, as demonstrated in the previous section, window observables have smaller reconstruction errors, which could otherwise hide discrepancies. Despite the limited control of lattice QCD systematics, the results are quite similar to the study from synthetic data. At larger n, the lattice results begin to lose signal as the observable becomes more akin to a pointlike reconstruction. The values at the smallest n have uncertainties comparable to phenomenology, demonstrating that precision benchmarking will become a possibility as lattice QCD results improve.

Conclusion and outlook—Hadrons are dynamic, strongly coupled systems composed of quarks and gluons. Asymptotic freedom ensures that the low-energy structure of hadrons can be factorized into universal, nonperturbative parton distribution functions.

A fundamental limitation of global analyses of parton distributions is the limited range of Bjorken-x available from experimental data. Similarly, a fundamental limitation of lattice QCD calculations is the limited range of noisy data. To benchmark lattice QCD calculations and to compare different approaches with phenomenological extractions, it is desirable to find observables with controlled errors. In this Letter, we propose one set of such observables, dubbed window observables. These quantities are sensitive to wide features in a region in x, allowing for more precise comparisons between lattice QCD results than point-by-point comparisons, while constrained to kinematic regions where global analyses are most reliable.

We demonstrate the extraction of the window observables from synthetic and real lattice data for the quark transversity of the nucleon, generated for a restricted range of Ioffe times. Lattice QCD results are most precise in low Fourier modes of the PDF, causing wider window observables to be dramatically more precise than suggested by a point-by-point comparison in x. In future calculations with data at multiple lattice spacings, pion masses, and physical volumes, the window observables will provide a high-precision tool for cross-validation of lattice QCD and phenomenology.

The software codes Chroma [53], QUDA [54,55], QPhiX [56], and Redstar [57] were used in our Letter.

Acknowledgments—We are grateful to Hervé Dutrieux for extensive discussions and helpful comments on the manuscript. This project was supported by the U.S. Department of Energy (DOE), Office of Science, Contract No. DE-AC05-06OR23177, under which Jefferson Science Associates, LLC operates Jefferson Lab. K. O. was supported in part by U.S. DOE Grant No. DE-FG02-04ER41302 and acknowledges the hospitality of the American Academy in Rome. This research was funded, in part (S. Z.), by l'Agence Nationale de la Recherche (ANR), Project No. ANR-23-CE31-0019. C. J. M. is supported in part by U.S. DOE Grant No. DE-SC0025908 and in part by U.S. DOE ECA No. DE-SC0023047. This work has benefited from the collaboration enabled by the Quark-Gluon Tomography (QGT) Topical Collaboration, U.S. DOE Award No. DE-SC0023646. Computations for this work were carried out in part on facilities of the USQCD Collaboration, which are funded by the Office of Science of the U.S. Department of Energy. The authors acknowledge William & Mary Research Computing for providing computational resources and/or technical support, which were provided by contributions from the National Science Foundation (MRI Grant No. PHY-1626177), and the Commonwealth of Virginia Equipment Trust Fund. In addition, this work used resources at NERSC, a DOE Office of Science User Facility supported by the Office of Science of the U.S. Department of Energy under Contract No. DE-AC02-05CH11231, as well as resources of the Oak Ridge Leadership Computing Facility at the Oak Ridge National Laboratory, which is supported by the Office of Science of the U.S. Department of Energy under Contract No. DE-AC05-00OR22725. The authors acknowledge support as well as computing and storage resources by

GENCI on Adastra (CINES), Jean-Zay (IDRIS) under Project No. (2020-2024)-A0080511504. The authors acknowledge support from the U.S. Department of Energy, Office of Science, Office of Advanced Scientific Computing Research and Office of Nuclear Physics, Scientific Discovery through Advanced Computing (SciDAC) program, and of the U.S. Department of Energy Exascale Computing Project (ECP). The authors also acknowledge the Texas Advanced Computing Center (TACC) at The University of Texas at Austin for providing HPC resources, like Frontera computing system [58] that has contributed to the research results reported within this Letter.

Data availability—The data that support the findings of this article are not publicly available because they are owned by a third party and the terms of use prevent public distribution. The data are available from the authors upon reasonable request.

[1] Y. Aoki *et al.* (Flavour Lattice Averaging Group (FLAG) Collaboration), FLAG review 2024, Reports No. CERN-TH-2024-192, FERMILAB-PUB-24-0785-T, 2024, arXiv:2411.04268.
[2] T. Aoyama *et al.*, The anomalous magnetic moment of the muon in the standard model, Phys. Rep. **887**, 1 (2020).
[3] V. Braun and D. Müller, Exclusive processes in position space and the pion distribution amplitude, Eur. Phys. J. C **55**, 349 (2008).
[4] A. V. Radyushkin, Quasi-parton distribution functions, momentum distributions, and pseudo-parton distribution functions, Phys. Rev. D **96**, 034025 (2017).
[5] Y.-Q. Ma and J.-W. Qiu, Exploring partonic structure of hadrons using ab initio lattice QCD calculations, Phys. Rev. Lett. **120**, 022003 (2018).
[6] X. Ji, Parton physics on a Euclidean lattice, Phys. Rev. Lett. **110**, 262002 (2013).
[7] A. Accardi *et al.*, Electron Ion Collider: The next QCD frontier: Understanding the glue that binds us all, Eur. Phys. J. A **52**, 268 (2016).
[8] A. Accardi *et al.*, Strong interaction physics at the luminosity frontier with 22 GeV electrons at Jefferson Lab, Eur. Phys. J. A **60**, 173 (2024).
[9] J. Karpie, K. Orginos, A. Rothkopf, and S. Zafeiropoulos, Reconstructing parton distribution functions from Ioffe time data: From Bayesian methods to neural networks, J. High Energy Phys. 04 (2019) 057.
[10] J. Liang, T. Draper, K.-F. Liu, A. Rothkopf, and Y.-B. Yang (XQCD Collaboration), Towards the nucleon hadronic tensor from lattice QCD, Phys. Rev. D **101**, 114503 (2020).
[11] L. Del Debbio, T. Giani, J. Karpie, K. Orginos, A. Radyushkin, and S. Zafeiropoulos, Neural-network analysis of parton distribution functions from Ioffe-time pseudodistributions, J. High Energy Phys. 02 (2021) 138.
[12] K. Cichy, L. Del Debbio, and T. Giani, Parton distributions from lattice data: The nonsinglet case, J. High Energy Phys. 10 (2019) 137.
[13] T. Khan, T. Liu, and R. S. Sufian, Gluon helicity in the nucleon from lattice QCD and machine learning, Phys. Rev. D **108**, 074502 (2023).
[14] T. A. Chowdhury, T. Izubuchi, M. Kamruzzaman, N. Karthik, T. Khan, T. Liu, A. Paul, J. Schoenleber, and R. S. Sufian, Polarized and unpolarized gluon PDFs: Generative machine learning applications for lattice QCD matrix elements at short distance and large momentum, Phys. Rev. D **111**, 074509 (2025).
[15] C. Alexandrou, G. Iannelli, K. Jansen, and F. Manigrasso (Extended Twisted Mass Collaboration), Parton distribution functions from lattice QCD using Bayes-Gauss-Fourier transforms, Phys. Rev. D **102**, 094508 (2020).
[16] A. Candido, L. Del Debbio, T. Giani, and G. Petrillo, Bayesian inference with Gaussian processes for the determination of parton distribution functions, Eur. Phys. J. C **84**, 716 (2024).
[17] H. Dutrieux, J. Karpie, K. Orginos, and S. Zafeiropoulos, Simple nonparametric reconstruction of parton distributions from limited Fourier information, Phys. Rev. D **111**, 034515 (2025).
[18] H. Dutrieux, J. Karpie, C. J. Monahan, K. Orginos, A. Radyushkin, D. Richards, and S. Zafeiropoulos, Inverse problem in the LaMET framework, arXiv:2504.17706.
[19] J. Karpie, K. Orginos, A. Radyushkin, and S. Zafeiropoulos (HadStruc Collaboration), The continuum and leading twist limits of parton distribution functions in lattice QCD, J. High Energy Phys. 11 (2021) 024.
[20] T. Blum, P. A. Boyle, V. Gülpers, T. Izubuchi, L. Jin, C. Jung, A. Jüttner, C. Lehner, A. Portelli, and J. T. Tsang (RBC, UKQCD Collaborations), Calculation of the hadronic vacuum polarization contribution to the muon anomalous magnetic moment, Phys. Rev. Lett. **121**, 022003 (2018).
[21] H.-W. Lin *et al.*, Parton distributions and lattice QCD calculations: A community white paper, Prog. Part. Nucl. Phys. **100**, 107 (2018).
[22] M. Constantinou *et al.*, Parton distributions and lattice-QCD calculations: Toward 3D structure, Prog. Part. Nucl. Phys. **121**, 103908 (2021).
[23] L. Gamberg, M. Malda, J. A. Miller, D. Pitonyak, A. Prokudin, and N. Sato (Jefferson Lab Angular Momentum (JAM) Collaboration), Updated QCD global analysis of single transverse-spin asymmetries: Extracting H^{-}, and the role of the Soffer bound and lattice QCD, Phys. Rev. D **106**, 034014 (2022).
[24] C. Cocuzza, A. Metz, D. Pitonyak, A. Prokudin, N. Sato, and R. Seidl (JAM Collaboration), Transversity distributions and tensor charges of the nucleon: Extraction from dihadron production and their universal nature, Phys. Rev. Lett. **132**, 091901 (2024).
[25] C. Cocuzza, A. Metz, D. Pitonyak, A. Prokudin, N. Sato, and R. Seidl (Jefferson Lab Angular Momentum (JAM) Collaboration), First simultaneous global QCD analysis of dihadron fragmentation functions and transversity parton distribution functions, Phys. Rev. D **109**, 034024 (2024).
[26] C. Egerer *et al.* (HadStruc Collaboration), Transversity parton distribution function of the nucleon using the pseudodistribution approach, Phys. Rev. D **105**, 034507 (2022).

[27] B. U. Musch, P. Hagler, J. W. Negele, and A. Schafer, Exploring quark transverse momentum distributions with lattice QCD, Phys. Rev. D **83**, 094507 (2011).

[28] V. Braun, P. Gornicki, and L. Mankiewicz, Ioffe—time distributions instead of parton momentum distributions in description of deep inelastic scattering, Phys. Rev. D **51**, 6036 (1995).

[29] B. L. Ioffe, Space-time picture of photon and neutrino scattering and electroproduction cross-section asymptotics, Phys. Lett. **30B**, 123 (1969).

[30] A. Radyushkin, One-loop evolution of parton pseudo-distribution functions on the lattice, Phys. Rev. D **98**, 014019 (2018).

[31] J.-H. Zhang, J.-W. Chen, and C. Monahan, Parton distribution functions from reduced Ioffe-time distributions, Phys. Rev. D **97**, 074508 (2018).

[32] T. Izubuchi, X. Ji, L. Jin, I. W. Stewart, and Y. Zhao, Factorization theorem relating Euclidean and light-cone parton distributions, Phys. Rev. D **98**, 056004 (2018).

[33] Z.-Y. Li, Y.-Q. Ma, and J.-W. Qiu, Extraction of next-to-next-to-leading-order parton distribution functions from lattice QCD calculations, Phys. Rev. Lett. **126**, 072001 (2021).

[34] J. Collins, *Foundations of Perturbative QCD*, Cambridge Monographs on Particle Physics, Nuclear Physics and Cosmology (Cambridge University Press, Cambridge, England, 2011).

[35] X. Ji, Y.-S. Liu, Y. Liu, J.-H. Zhang, and Y. Zhao, Large-momentum effective theory, Rev. Mod. Phys. **93**, 035005 (2021).

[36] J. Karpie, K. Orginos, and S. Zafeiropoulos, Moments of Ioffe time parton distribution functions from non-local matrix elements, J. High Energy Phys. 11 (2018) 178.

[37] Z. Pang, J.-H. Zhang, and D.-J. Zhao, Moments from momentum derivatives in lattice QCD, Chin. Phys. C **49**, 101001 (2025).

[38] S. Forte and L. Magnea, Truncated moments of parton distributions, Phys. Lett. B **448**, 295 (1999).

[39] S. Forte, L. Magnea, A. Piccione, and G. Ridolfi, Evolution of truncated moments of singlet parton distributions, Nucl. Phys. **B594**, 46 (2001).

[40] A. Piccione, Solving the Altarelli-Parisi equations with truncated moments, Phys. Lett. B **518**, 207 (2001).

[41] D. Kotlorz and A. Kotlorz, Evolution equations for truncated moments of the parton distributions, Phys. Lett. B **644**, 284 (2007).

[42] A. Psaker, W. Melnitchouk, M. E. Christy, and C. Keppel, Quark-hadron duality and truncated moments of nucleon structure functions, Phys. Rev. C **78**, 025206 (2008).

[43] E. C. Aschenauer, R. Sassot, and M. Stratmann, Helicity parton distributions at a future electron-ion collider: A quantitative appraisal, Phys. Rev. D **86**, 054020 (2012).

[44] D. Kotlorz and A. Kotlorz, Evolution of the truncated Mellin moments of the parton distributions in QCD analysis, Phys. Part. Nucl. Lett. **11**, 357 (2014).

[45] D. Kotlorz and S. V. Mikhailov, Cut moments and a generalization of DGLAP equations, J. High Energy Phys. 06 (2014) 065.

[46] D. Kotlorz and A. Kotlorz, Analysis of DIS structure functions of the nucleon within truncated Mellin moments approach, Int. J. Mod. Phys. A **31**, 1650181 (2016).

[47] C. Egerer, D. Richards, and F. Winter, Controlling excited-state contributions with distillation in lattice QCD calculations of nucleon isovector charges g_S^{u-d}, g_A^{u-d}, g_T^{u-d}, Phys. Rev. D **99**, 034506 (2019).

[48] G. Martinelli, C. Pittori, C. T. Sachrajda, M. Testa, and A. Vladikas, A general method for nonperturbative renormalization of lattice operators, Nucl. Phys. **B445**, 81 (1995).

[49] C. Sturm, Y. Aoki, N. H. Christ, T. Izubuchi, C. T. C. Sachrajda, and A. Soni, Renormalization of quark bilinear operators in a momentum-subtraction scheme with a non-exceptional subtraction point, Phys. Rev. D **80**, 014501 (2009).

[50] S. Park, R. Gupta, B. Yoon, S. Mondal, T. Bhattacharya, Y.-C. Jang, B. Joó, and F. Winter (Nucleon Matrix Elements (NME) Collaoration), Precision nucleon charges and form factors using (2 + 1)-flavor lattice QCD, Phys. Rev. D **105**, 054505 (2022).

[51] J. A. Gracey, RI′/SMOM scheme amplitudes for quark currents at two loops, Eur. Phys. J. C **71**, 1567 (2011).

[52] B. Yoon *et al.*, Isovector charges of the nucleon from 2 + 1-flavor QCD with clover fermions, Phys. Rev. D **95**, 074508 (2017).

[53] R. G. Edwards and B. Joo (SciDAC, LHPC, UKQCD Collaborations), The Chroma software system for lattice QCD, Nucl. Phys. B, Proc. Suppl. **140**, 832 (2005).

[54] M. Clark, R. Babich, K. Barros, R. Brower, and C. Rebbi, Solving lattice QCD systems of equations using mixed precision solvers on GPUs, Comput. Phys. Commun. **181**, 1517 (2010).

[55] R. Babich, M. A. Clark, and B. Joo, Parallelizing the QUDA library for multi-GPU calculations in lattice quantum chromodynamics, in SC 10 (Supercomputing 2010) (2010), arXiv:1011.0024.

[56] B. Joó, D. D. Kalamkar, T. Kurth, K. Vaidyanathan, and A. Walden, Optimizing Wilson-Dirac operator and linear solvers for intel® KNL, in High Performance Computing: ISC High Performance 2016 International Workshops, ExaComm, E-MuCoCoS, HPC-IODC, IXPUG, IWOPH, P^3 MA, VHPC, WOPSSS, Frankfurt, Germany, 2016, Revised Selected Papers, edited by M. Taufer, B. Mohr, and J. M. Kunkel (Springer International Publishing, Cham, 2016), pp. 415–427.

[57] J. Chen, R. G. Edwards, and W. Mao, Graph contractions for calculating correlation functions in lattice QCD, in *Platform for Advanced Scientific Computing* (Association for Computing Machinery, New York, 2023).

[58] D. Stanzione, J. West, R. T. Evans, T. Minyard, O. Ghattas, and D. K. Panda, Frontera: The evolution of leadership computing at the National Science Foundation, in *Practice and Experience in Advanced Research Computing*, PEARC '20 (Association for Computing Machinery, New York, 2020), pp. 106–111.

End Matter

Window observables as Ioffe time integrals—The window observables can be written as integrals in Ioffe time. Let us start from the general convolution without bounds on x:

$$W_n(x_\pm) = \int_{-\infty}^{\infty} dx w_n(x; x_\pm) q(x) \tag{A1}$$

following the assumption that $q(|x| > 1) = 0$. The convolution theorem leads us to the analogous Fourier integration

$$W_n(x_\pm) = \int_{-\infty}^{\infty} \frac{d\nu}{2\pi} \tilde{w}_n(\nu; x_\pm) M(-\nu), \tag{A2}$$

where $\tilde{w}(\nu)$ is the inverse FT of $w(x)$.

The Gaussian window given in Eq. (10), which limits the range of x to the vicinity of the midpoint between $x_\pm$, has an inverse FT

$$\tilde{w}_n(\nu) = \exp\left[i\nu\frac{x_+ + x_-}{2} - \frac{(x_+ - x_-)^2\nu^2}{2n^2}\right], \tag{A3}$$

where n controls how localized the Gaussian is within the window $[x_-, x_+]$.

The window moment can be written using step functions θ:

$$a_n(x_-, x_+) = \int_{-\infty}^{\infty} dx[\theta(x - x_-) - \theta(x - x_+)]x^{n-1} q(x). \tag{A4}$$

For the integration bounds, there is an assumption that the PDF vanished outside the bounds of $x \in [-1, 1]$, or $x \in [0, 1]$ when CP projected, but with the limited bounds $|x_\pm| < 1$ used in practice this assumption does not matter. The step functions can be replaced by approximations such as a sigmoid or arctangent function, with limited modifications to the following derivation, but in the following we use Heaviside step functions.

Inserting the inverse Fourier transforms of q and θ, we obtain

$$a_n(x_-, x_+) = \int \frac{d\nu}{2\pi}(e^{ix_-\nu} - e^{ix_+\nu})\tilde{\theta}(\nu) \times \int \frac{d\nu'}{2\pi} M(\nu') \int dx x^{n-1} e^{-ix(\nu+\nu')}, \tag{A5}$$

where $\tilde{\theta}(\nu)$ is the inverse Fourier transform of $\theta(x)$:

$$\tilde{\theta}(\nu) = \pi\delta(\nu) - \frac{i}{\nu}. \tag{A6}$$

The x integrals can be evaluated as $\delta(\nu + \nu')$ or its derivatives

$$a_n(x_-, x_+) = \int \frac{d\nu d\nu'}{(2\pi)}(e^{ix_-\nu} - e^{ix_+\nu})\tilde{\theta}(\nu) \times M(\nu')(-i)^{n-1}\delta^{(n-1)}(\nu + \nu'). \tag{A7}$$

Given that the ITD converges to 0 as $\nu \to \infty$, one can integrate by parts so that derivatives of delta functions give derivatives of the ITD:

$$a_n(x_-, x_+) = i^{n-1} \int \frac{d\nu}{(2\pi)}(e^{ix_-\nu} - e^{ix_+\nu})\tilde{\theta}(\nu) M^{(n-1)}(-\nu). \tag{A8}$$

Inserting $\tilde{\theta}(\nu)$, the delta function term will vanish, since the phase terms cancel at $\nu = 0$ while the derivative of the ITD remains finite. The other term can be integrated by parts to give

$$a_n(x_-, x_+) = \frac{i^{n-2}}{4\pi^2} \int d\nu M(-\nu) \frac{\partial^{n-1}}{\partial\nu^{n-1}}\left[\frac{e^{ix_-\nu} - e^{ix_+\nu}}{\nu}\right]. \tag{A9}$$

For $n = 2$, this becomes

$$a_2(x_-, x_+) = \frac{1}{2\pi}\int \mathrm{d}\nu \frac{M(-\nu)}{\nu^2} \times \left[(ix_-\nu - 1)e^{ix_-\nu} - (ix_+\nu - 1)e^{ix_+\nu}\right]. \tag{A10}$$

The expression for general n is given by

$$a_n(x_-, x_+) = \frac{i^{n-2}}{2\pi} \int d\nu \frac{M(-\nu)}{\nu^n} \times \left[e^{ix_-\nu} p_{n-1}(ix_-\nu) - e^{ix_+\nu} p_{n-1}(ix_+\nu)\right], \tag{A11}$$

where

$$p_n(x) = -\sum_{k=0}^{n} \frac{n!}{k!}(-x)^k. \tag{A12}$$

The integrand in the general case is, therefore, suppressed by an additional power of ν compared to the integrands needed to obtain PDFs or pseudo-PDFs, which already decay with a power law based upon the low-x divergence [28]. In the limit of $\nu \to 0$, the integrand approaches

$$\frac{(x_-)^n - (x_+)^n}{2\pi n}, \tag{A13}$$

which vanishes for even n when $x_- = -x_+$. This exact value can be used as a fixed point to guide the interpolation and extrapolation of data required to perform the integral in ν space.

Relative error of JAM3D reconstructions*—Figure 5 shows the relative accuracy of the PDF and window observable reconstructions in Figs. 1 and 2. In the PDF reconstruction, the lower-x regime, specifically in the window studied $x \in [0.1, 0.5]$, systematically over estimates the error point by point. The lower-n window moment integrals, on the other hand, reconstruct the value with significantly less error than the point-by-point reconstruction would have implied. The lowest n actually reproduces the original error's size, while larger n give the systematic overestimation of point-by-point reconstruction.

Results from JAMDiFF—Figures 6 and 7 are the same as Figs. 1 and 2, respectively, except the synthetic data were generated with the JAMDiFF results. As constructed, the phenomenological CP-odd isovector $u - d$ transversity PDF q_+ has larger uncertainties at low x than those from JAM3D*. The reconstruction of the PDF from the imaginary component data results in an underestimation of this large uncertainty.

Results from JAM3D with* $\nu_{\max} = 10$—Figures 8 and 9 are the same as Figs. 1 and 2, respectively, with a $\nu_{\max} = 10$. The reconstruction error is significantly more under control. The window observables' errors are more similar to the true value, specifically for larger n.

Alternate choices of windows—This section shows the window observables for other choices of the window, $(x_-, x_+) = (0.1, 1)$, (0.3,0.5), and (0.1,0.3). Figure 10 shows the window moments, and Fig. 11 shows the Gaussian windows. Similar to the window chosen for

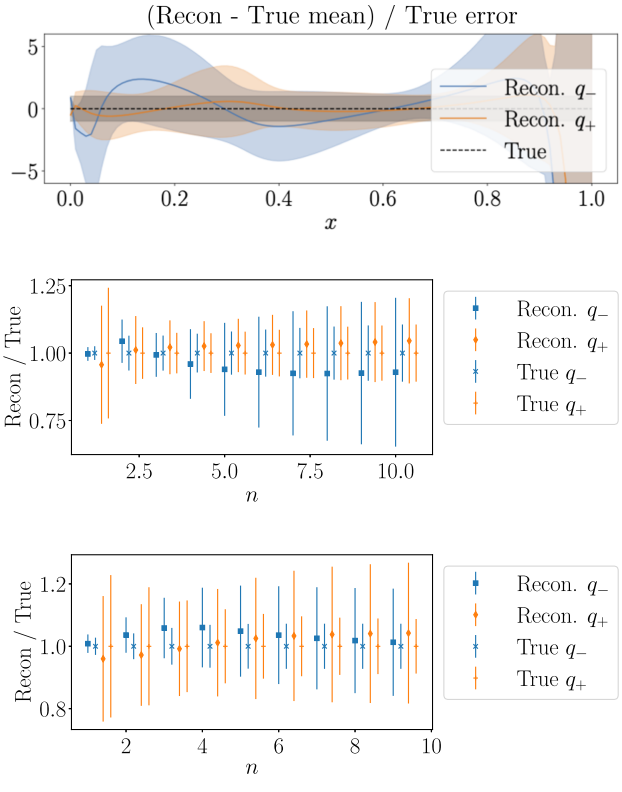


FIG. 5. The relative error in the reconstructions of the PDF (upper), window moments (middle), and Gaussian windows (lower).

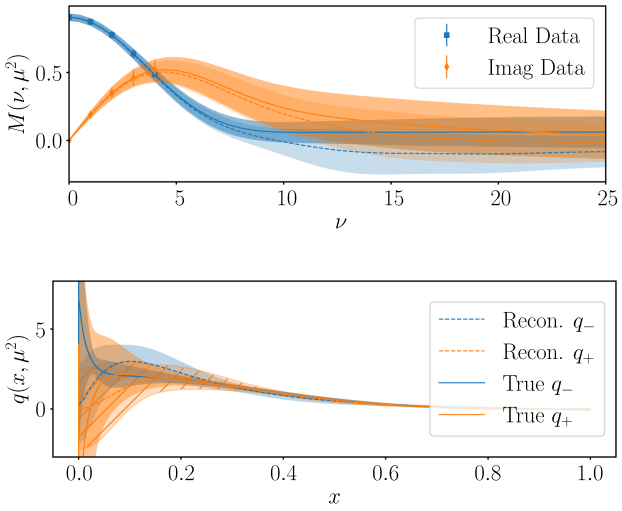


FIG. 6. The same as Fig. 1 except with data generated from JAMDiFF results except the reconstructed q_+ PDF is hatched for visibility.

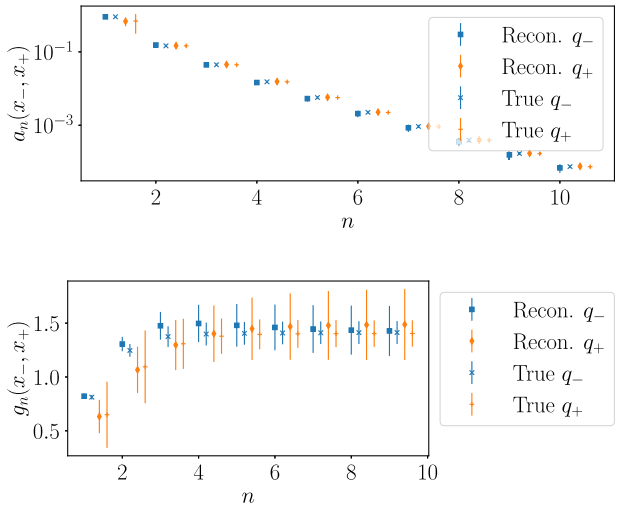


FIG. 7. The same as Fig. 2 with data generated from JAMDiFF results.

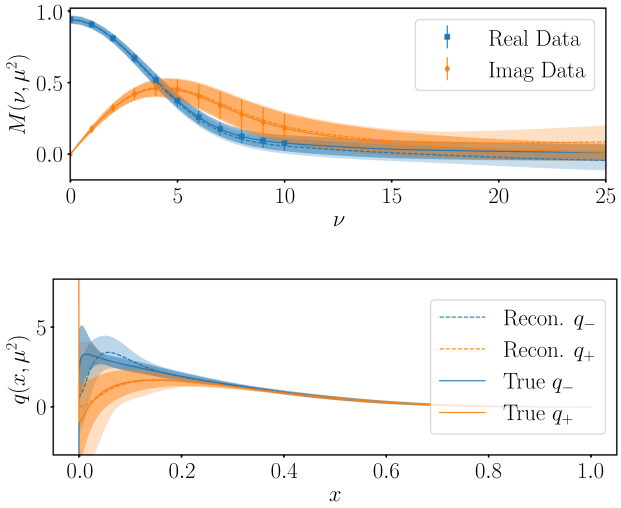


FIG. 8. The same as Fig. 1 except with $\nu_{\max} = 10$.

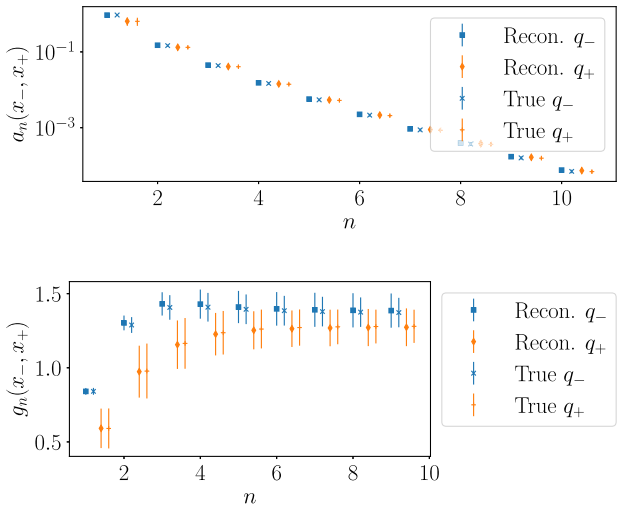


FIG. 9. The same as Fig. 2 except with $\nu_{\max} = 10$.

the main text, these show consistent reproduction from both real and imaginary components. At larger n, the error estimated from the synthetic data is overestimated, while smaller n tends to have more precise reproduction.

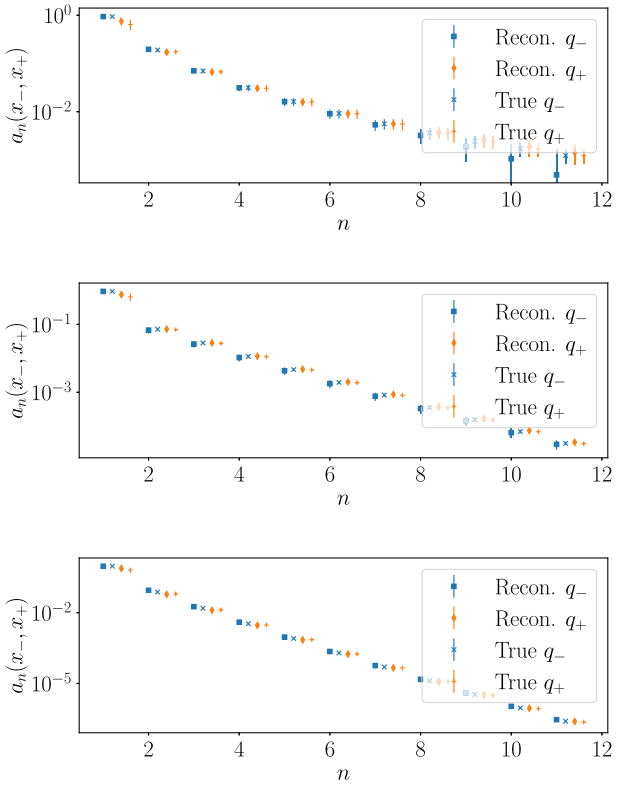


FIG. 10. The window moments with, in descending order, $(x_-, x_+) = (0.1, 1)$, (0.3, 0.5), and (0.1, 0.3).

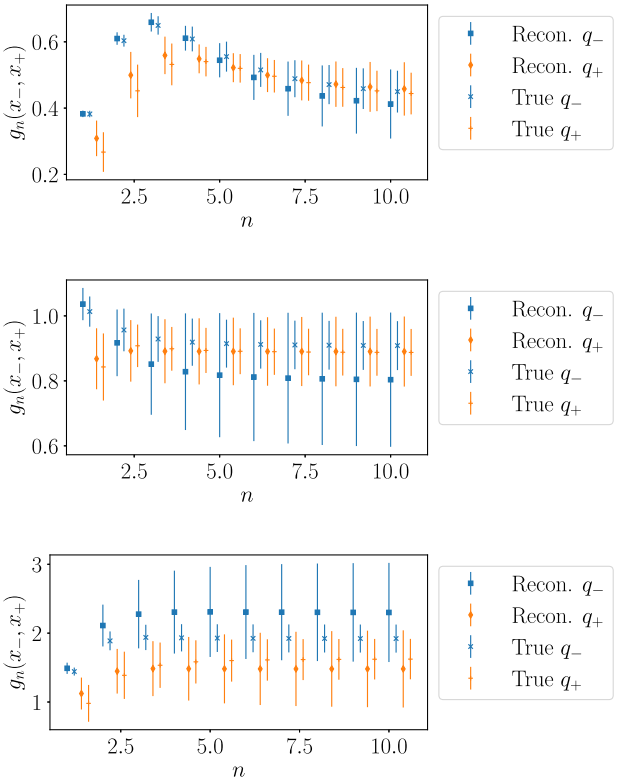


FIG. 11. The Gaussian windows with, in descending order, $(x_-, x_+) = (0.1, 1)$, (0.3, 0.5), and (0.1, 0.3).